

This article was downloaded by: [West Virginia University]

On: 10 March 2015, At: 12:10

Publisher: Taylor & Francis

Informa Ltd Registered in England and Wales Registered Number: 1072954 Registered office: Mortimer House, 37-41 Mortimer Street, London W1T 3JH, UK



[Click for updates](#)

Journal of Biomolecular Structure and Dynamics

Publication details, including instructions for authors and subscription information:
<http://www.tandfonline.com/loi/tbsd20>

Rich Spectroscopic and Molecular Dynamic Studies on the Interaction of Cytotoxic Pt(II) and Pd(II) Complexes of Glycine derivatives with Calf Thymus DNA

Mahboube Eslami Moghadam^a, Maryam Saidifar^b, Adeleh Divsalar^c, Hassan Mansouri-Torshizi^d, Ali-Akbar Saboury^e, Hossein Farhangian^a & Maryam Ghadamgahi^f

^a Chemistry & Chemical Engineering Research Center of Iran, Tehran, Iran

^b Nanotechnology and Advanced Materials Department, Materials and Energy Research Center, Karaj, Iran

^c Department of Biological Sciences, Kharazmi (Tarbiat Moallem) University, Tehran, Iran

^d Department of Chemistry, University of Sistan & Baluchestan, Zahedan, Iran

^e Institute of Biochemistry and Biophysics, University of Tehran, Tehran, Iran

^f School of Chemistry, Damghan University, Damghan, Iran

Accepted author version posted online: 03 Mar 2015.

To cite this article: Mahboube Eslami Moghadam, Maryam Saidifar, Adeleh Divsalar, Hassan Mansouri-Torshizi, Ali-Akbar Saboury, Hossein Farhangian & Maryam Ghadamgahi (2015): Rich Spectroscopic and Molecular Dynamic Studies on the Interaction of Cytotoxic Pt(II) and Pd(II) Complexes of Glycine derivatives with Calf Thymus DNA, *Journal of Biomolecular Structure and Dynamics*, DOI: [10.1080/07391102.2015.1015056](https://doi.org/10.1080/07391102.2015.1015056)

To link to this article: <http://dx.doi.org/10.1080/07391102.2015.1015056>

Disclaimer: This is a version of an unedited manuscript that has been accepted for publication. As a service to authors and researchers we are providing this version of the accepted manuscript (AM). Copyediting, typesetting, and review of the resulting proof will be undertaken on this manuscript before final publication of the Version of Record (VoR). During production and pre-press, errors may be discovered which could affect the content, and all legal disclaimers that apply to the journal relate to this version also.

PLEASE SCROLL DOWN FOR ARTICLE

Taylor & Francis makes every effort to ensure the accuracy of all the information (the "Content") contained in the publications on our platform. However, Taylor & Francis, our agents, and our licensors make no representations or warranties whatsoever as to the accuracy, completeness, or suitability for any purpose of the Content. Any opinions and views expressed in this publication are the opinions and views of the authors, and are not the views of or endorsed by Taylor & Francis. The accuracy of the Content should not be relied upon and should be independently verified with primary sources of information. Taylor and Francis shall not be liable for any losses, actions, claims, proceedings, demands, costs, expenses, damages, and other liabilities whatsoever or howsoever caused arising directly or indirectly in connection with, in relation to or arising out of the use of the Content.

This article may be used for research, teaching, and private study purposes. Any substantial or systematic reproduction, redistribution, reselling, loan, sub-licensing, systematic supply, or distribution in any form to anyone is expressly forbidden. Terms & Conditions of access and use can be found at <http://www.tandfonline.com/page/terms-and-conditions>

Publisher: Taylor & Francis

Journal: *Journal of Biomolecular Structure and Dynamics*

DOI: <http://dx.doi.org/10.1080/07391102.2015.1015056>

Rich Spectroscopic and Molecular Dynamic Studies on the Interaction of Cytotoxic Pt(II) and Pd(II) Complexes of Glycine derivatives with Calf Thymus DNA

Mahboube Eslami Moghadam^{1,*}, Maryam Saidifar², Adeleh Divsalar³, Hassan Mansouri-Torshizi⁴, Ali-Akbar Saboury⁵, Hossein Farhangian¹ and Maryam Ghadamgahi⁶

¹*Chemistry & Chemical Engineering Research Center of Iran, Tehran, Iran*

²*Nanotechnology and Advanced Materials Department, Materials and Energy Research Center, Karaj, Iran*

³*Department of Biological Sciences, Kharazmi (Tarbiat Moallem) University, Tehran, Iran*

⁴*Department of Chemistry, University of Sistan & Baluchestan, Zahedan, Iran*

⁵*Institute of Biochemistry and Biophysics, University of Tehran, Tehran, Iran*

⁶*School of Chemistry, Damghan University, Damghan, Iran*

* Corresponding author. Tel.: +98 21 44580772; fax: +98 21 44580753; e-mail:

eslami_moghadam@ccerci.ac.ir & eslami_moghadam@yahoo.com

Rich Spectroscopic and Molecular Dynamic Studies on the Interaction of Cytotoxic Pt(II) and Pd(II) Complexes of Glycine derivatives with Calf Thymus DNA

Abstract

Some amino acid derivatives, such as R-glycine, have been synthesized together with their full spectroscopic characterization. The sodium salts of these bidentate amino acid ligands have been interacted with $[M(\text{bpy})(\text{H}_2\text{O})_2](\text{NO}_3)_2$ giving the corresponding some new complexes with formula $[M(\text{bpy})(\text{R-gly})]\text{NO}_3$ (where M is Pt(II) or Pd(II), bpy is 2,2'-bipyridine and R-gly is butyl-, hexyl- and octyl-glycine). Due to less solubility of octyl derivatives, the biological activities of butyl and hexyl derivatives have been tested against chronic myelogenous leukemia cell line, K562. The interaction of these complexes with highly polymerized calf thymus DNA has been extensively studied by means of electronic absorption, fluorescence and other measurements. The experimental results suggest that these complexes positive cooperatively bind to DNA presumably via groove binding. Molecular dynamic results show that the DNA structure is largely maintained its native structure in hexylglycine derivative–water mixtures and at lower temperatures. The simulation data indicates that the more destabilizing effect of butylglycine is induced by preferential accumulation of these molecules around the DNA and due to their more negative free energy of binding via groove binding.

Keywords: Platinum and palladium complexes; Cytotoxicity; Amino acid derivative; Calf thymus DNA; Molecular dynamics simulation.

List of abbreviations

protein data bank (PDB)

Particle-Mesh Ewald (PME)

molecular dynamic (MD)

root mean square deviation (RMSD)

gyration radius (Rg)

hydrogen bonds (H-B)

radial distribution function (RDF)

Introduction

Design and synthesis of new cisplatin analogs, as potential anticancer drugs, have been renewed by the utilization of bidentate ligands in the development and the treatment of cancer (1). Cisplatin has been used in the treatment of testicular cancers, and solid malignancies such as bone, neck and bladder cancers (2). Due to the dose limiting toxic side-effects of cisplatin, much current research work is aimed at the discovery of platinum complexes which are not cross-resistant with cisplatin, have fewer toxic side-effects, are active against a broad range of types of cancer and can be administered orally (3-7). In response to these needs, one approach is using a variety of amino acids as ligands.

Several water soluble platinum and palladium complexes with bidentate essential amino acids have been reported (8-14). These complexes have shown anticancer activity comparable to or greater than cisplatin. Also suggested that the palladium complexes may be useful for the treatment of tumors of the gastrointestinal region where cisplatin fails (2).

In addition, the substitution of chloride ligands of cisplatin or its palladium analogs with bidentate ligands such as amino acid or amino acid derivatives that are found in biological systems may decrease their toxic side effects or increase the concentration of drug inside the cell and thus improve the antitumor activities of these agents (15). It has been reported that many active complexes could react with DNA and inhibit its synthesis (16,17). Recently, several platinum complexes of diamine chelating ligands bearing amino-acid type substituents have been reported (18). They have been interacted with a mononucleotide and DNA. Their results suggested that the presence of different amino acids derivatives in these complexes can modulate their solubility and cytotoxic activity. We have earlier reported the synthesis, characterization and protein binding studies of a Pd(II) complex bearing amino acid derivative (19). The present study deals with synthesis and characterization of some novel mixed-ligand platinum(II) and palladium(II) complexes of 2,2'-bipyridine and amino acid derivatives (see scheme 1) including *in vitro* anti-tumor and detail calf thymus DNA binding studies. Computer simulations can examine these interactions and describe important features for DNA-

ligand recognition (20). MD simulation has been applied to evaluate the binding of newly mentioned complexes to DNA. The LIE algorithm has been applied to calculate and compare the binding free energies of DNA-ligand systems (21).

Experimental

Materials and Methods

Octylamine, hexylamine, butylamine, sodium chloride, sodium bicarbonate, sodium hydroxide, hydrochloric acid, sulfuric acid, potassium tetrachloroplatinate, 2,2'-bipyridine, highly polymerized calf thymus DNA sodium salt and Tris-HCl buffer were purchased from Merck (Germany). Palladium(II) chloride anhydrous was obtained from Fluka (Switzerland). Bromo acetic acid, carbon disulfide and ethidium bromide were obtained from Aldrich (England). [Pt(bpy)Cl₂] and [Pd(bpy)Cl₂] were prepared according to the literature procedure (22). Solvents were purified prior to use by the standard procedures. Other chemicals used were of analytical reagent or higher purity grade.

The melting points of the compounds were determined on a Unimelt capillary melting point apparatus and reported as they were. Infrared spectra (4000-400 cm⁻¹) were determined in KBr disks on a JASCO-460 plus FT-IR spectrophotometer. UV-Vis spectra were recorded on a JASCO UV/VIS-7850 recording spectrophotometer. ¹H NMR spectra were measured on a Bruker DRX-500 Avance spectrometer at 500 MHz, using TMS as the internal reference in DMSO-d₆. The fluorescence spectra were carried out on a Hitachi MPF-4 spectrofluorimeter. Conductivity measurements of the above platinum and palladium complexes were carried out on a Systronics Conductivity Bridge 305, using a conductivity cell of cell constant 1.0 and doubly distilled water was used as solvent. Carbon, hydrogen and nitrogen in the ligand and the complexes were analyzed on a Herause CHNO-RAPID elemental analyzer.

Synthesis of Ligands and Metal Complexes

Synthesis of Butylglycine, Hexylglycine and Octylglycine

To a solution of bromoethylacetate (6 mL, 53 mmol) in benzene (10 mL), a solution of Alkyl amine (106 mmol) in benzene (40 mL) was added dropwise with constant stirring (19). The reaction mixture was refluxed for two hours and then cooled. The

amine hydrobromide was filtered off, washed with small amount of benzene and discarded. From the combined filtrate, all the benzene was removed by rotaevaporator until a white fume was observed. 2.12 g sodium hydroxide (53 mmol) in 8 ml distilled water was added, refluxed for 30 min. and cooled. The solution was transferred to a separator funnel and washed with diethyl ether (two times, each time 20 mL) to remove undesired organic materials. The aqueous layer was acidified with HCl to pH=2 and slowly evaporated at 35 °C until crystals appeared and left aside for 24 h.

Recrystallization was carried out by dissolving the filtered crystals in minimum amount of distilled water, acidifying to pH=2, and slow evaporation. The pure crystals so obtained was filtered and dried in a desiccator under vacuum over KOH pellets. This reaction proceeds in accord with Scheme 2.

Butylglycine ($CH_3-(CH_2)_3-NH-CH_2-COOH.HCl$), Yield: 80% with a melting point of 199-201 °C. Analytical calculated for $C_6H_{14}NO_2Cl$ (167.5): C, 42.98; H, 8.36; N, 8.36. Analytical found: C, 42.95; H, 8.33; N, 8.4%; IR (cm^{-1} , solid): 3415(w, O-H), 2942(w, N-H), 2813(w, C-H), 1766 (s, C=O), 1208(s, C-O). 1H NMR (300 MHz, DMSO- d_6 , δ in ppm, J in MHz): 0.85 (t, 3H, 18.75), 1.28 (m, 2H), 1.6 (m, 2H), 2.86 (m, 2H), 3.78 (s, 2H), 9.3 (sb, NH and OH).

Hexylglycine ($CH_3-(CH_2)_5-NH-CH_2-COOH.HCl$), Yield: 69% with a melting point of 206-208 °C. Analytical calculated for $C_8H_{18}NO_2Cl$ (195.5): C, 49.10; H, 9.20; N, 7.16. Analytical found: C, 49.08; H, 9.18; N, 7.15%; IR (cm^{-1} , solid): 3412(w, O-H), 2946(w, N-H), 2829(w, C-H), 1752(s, C=O), 1215(s, C-O); 1H NMR (300 MHz, DMSO- d_6 , δ in ppm, J in MHz): 0.875 (t, 3H, 12.11), 1.338 (m, 6H), 1.57 (m, 2H), 2.81 (m, 2H), 3.85 (s, 2H), 9.35 (sb, NH and OH).

Octylglycine ($CH_3-(CH_2)_7-NH-CH_2-COOH.HCl$), Yield: 81% with a melting point of 216-217 °C. Analytical calculated for $C_{10}H_{22}NO_2Cl$ (225.5): C, 52.6; H, 9.7; N, 6.0. Analytical found: C, 52.6; H, 9.6; N, 6.0%; IR (cm^{-1} , solid): 3400 (w, O-H), 2950 (w, N-H), 2900 (w, C-H), 1740 (s, C=O), 1220 (s, C-O); 1H NMR (300 MHz, DMSO- d_6 , δ in ppm): 0.86 (t, 3H, 6.193), 1.25(m, 10H), 1.64(m, 2H), 2.87(t, 2H, 7.80), 3.8 (s, 2H), 9.3 (sb, NH and OH).

Synthesis of [Pt/Pd(bpy)(Butylgly)]NO₃ complexes

1 mmol of [Pt(bpy)Cl₂] or [Pd(bpy)Cl₂] was suspended in 120 mL of doubly distilled water. To this solution, 0.34 mg of AgNO₃ (2 mmol) in 20 mL water was added slowly

with continuous stirring. The reaction mixture was heated for 7 h at 75 °C and then for 15 h at room temperature under dark with constant stirring. The AgCl precipitate was removed by filtering through Whatman filter paper No.42. This filtrate at 50 °C was mixed with butyl-glycine hydrochloride (0.17 g, 1 mmol) and NaHCO₃ (0.17 g, 2 mmol) dissolved in 10 mL distilled water. The reaction mixture was further stirred and concentrated at 50 °C for 45 min. to 60 mL and then cooled. The trace amount of turbidity formed was filtered and the clear yellow filtrate was further concentrated to about 5 mL at 35 °C (very fine needle crystals of the complex not suitable for X-Ray crystallography were obtained by slow evaporation of this solution). The crystals formed was filtered and washed with little amount of chilled double distilled water and then dried in an oven at 45 °C.

[Pt(bpy)(Butylgly)]NO₃: Yield: 48% and decomposes at 205-207 °C. Analytical calculated for C₁₆H₂₀N₄O₅Pt (544): C, 35.36; H, 3.68; N, 10.31%. Analytical found: C, 35.4; H, 3.65; N, 10.33%; UV Band maxima in nm (ϵ_M in liter mole⁻¹ cm⁻¹ × 10⁻⁴): 363(0.37), 321(0.85), 310(0.73), 283(1.36), 207(3.23); IR (cm⁻¹, solid): 3435 (w, N-H), 3048 (w), 2903 (w), 1680 (s, C=O), 1607 and 1471 (s, C=C), 1384 (s, NO₃⁻); ¹H NMR (300 MHz, DMSO-d₆, δ in ppm, J in MHz): 0.8 (t, 3H, 12.5), 1.34(m, 2H), 1.75,1.95(m, 2H, 143.7), 2.89,2.98(m, 2H, 68.75), 3.47,4.96(m, 2H, 468.7), 8.45(s, NH), Aromatic protons: 7.85(d, 2H), 8.49(t, 2H), 8.64(m, 2H); Molar conductance of 0.06 mM aqueous solution: 120 cm²ohm⁻¹mol⁻¹.

[Pd(bpy)(Butylgly)]NO₃: Yield: 41% and decomposes at 197.7-198.9 °C. Analytical calculated for C₁₆H₂₀N₄O₅Pd (455): C, 42.29; H, 4.41; N, 12.33%. Analytical calculated for: C, 42.34; H, 4.44; N, 12.30%; UV Band maxima in nm (ϵ_M in liter mole⁻¹ cm⁻¹ × 10⁻⁴): 309 (0.98), 239 (1.22), 207 (4.02); IR (cm⁻¹, solid): 3434 (w, N-H), 3080 (w), 2923 (w), 1673 (s, C=O), 1602 and 1466 (s, C=C), 1384 (s, NO₃⁻); ¹H NMR (300 MHz, DMSO-d₆, δ in ppm, J in MHz): 0.87 (t, 3H, 12.5), 1.37 (m, 2H), 1.82,2(m, 2H, 187.5), 2.83, 2.92(m, 2H, 62.5), 3.26,4.15(m, 2H, 718.7), 6.71(s, NH), Aromatic protons: 7.87(d, 2H), 8.65(m, 4H), 9.04(m, 2H); Molar conductance of 0.06 mM aqueous solution: 136 cm²ohm⁻¹mol⁻¹.

[Pt(bpy)(hexylgly)]NO₃: Yield: 45% and decomposes at 187.3-188.6 °C; Analytical calculated for C₁₈H₂₄N₄O₅Pt (572): C, 37.83; H, 4.20; N, 9.81%. Analytical calculated for: C, 37.86; H, 4.25; N, 9.88%; UV Band maxima in nm (ϵ_M in liter mole⁻¹ cm⁻¹ × 10⁻⁴): 341(0.25), 318(1.29), 306(1.07), 247(1.97), 202(2.49); IR (cm⁻¹, solid): 3435 (w, N-

H), 3113 (w), 2929 (w), 1677 (s, C=O), 1602 and 1470 (s, C=C), 1384 (s, NO₃); ¹H NMR (300 MHz, DMSO-d₆, δ in ppm, J in MHz): 0.8 (t, 3H, 12.5), 1.22 (m, 4H), 1.31 (m, 2H), 1.75, 1.95 (m, 2H, 200), 2.9, 2.98 (m, 2H, 50), 3.47, 3.95 (m, 2H, 375), 7.95 (s, NH), Aromatic protons: 7.87 (m, 2H), 8.47 (m, 2H), 8.7 (m, 2H), 8.9 (d, 2H); Molar conductance of 0.04 mM aqueous solution: 124.2 cm²ohm⁻¹mol⁻¹.

[Pd(bpy)(hexylgly)]NO₃ and [Pd(bpy)(octylgly)]NO₃ were synthesized by a method similar to one described previously (19).

[Pt(bpy)(ocylgly)]NO₃: Yield: 41% and decomposes at 186.6-188.4 °C; Analytical calculated for C₂₀H₂₈N₄O₅Pt (600): C, 40.07; H, 4.67; N, 9.35%. Analytical calculated for: C, 40.12; H, 4.69; N, 9.30%; UV Band maxima in nm (ε_M in liter mole⁻¹ cm⁻¹ × 10⁻⁴): 366(0.38), 321(0.72), 309(0.67), 285(1.17), 207(2.73); IR (cm⁻¹, solid): 3435 (w, N-H), 3118 (w), 2924 (w), 1677 (s, C=O), 1609 and 1467 (s, C=C), 1394 (s, NO₃); ¹H NMR (300 MHz, DMSO-d₆, δ in ppm, J in MHz): 0.79 (t, 3H, 12.5), 1.95 (m, 8H), 1.32 (m, 2H), 1.74, 1.93 (m, 2H, 200), 2.91, 2.98 (m, 2H, 50), 3.53, 3.98 (m, 2H, 500), 7.67 (s, NH), Aromatic protons: 7.88 (m, 2H), 8.49 (m, 2H), 8.67 (m, 2H), 8.78 (d, 2H); Molar conductance of 0.05 mM aqueous solution: 123 cm²ohm⁻¹mol⁻¹.

Cell culture

Human tumor cell line K562 (which was obtained from National Cell Bank of Iran (NCBI)-Pasteur Institute of Iran), was selected for study of various Pd(II) complexes cytotoxicity. Cells were grown in the RPMI medium (RPMI, Sigma). The medium was supplemented with L-glutamine (2 mM), streptomycin and penicillin (5 μg/mL) and 10% heat-inactivated fetal calf serum, at 37 °C under a 5% CO₂ / 95% air atmosphere.

In vitro cytotoxicity study

The *in vitro* cytotoxicity was studied using the MTT assay. The cleavage and the conversion of the soluble yellowish MTT to the insoluble purple formazan by active mitochondrial dehydrogenase of living cells had been used to develop an assay system alternative to other assays for measurement of cell proliferation. Harvested cells were seeded into a 24-well plate (2 × 10⁵ cell/ml) with different amounts of free Pd(II) complexes (0-240 μM) for 24 h. Four hours to the end of the incubations, 50 μL of MTT solution (5 mg/mL in PBS) was added to each well containing fresh and cultured medium. At the end of the incubation, the insoluble formazan produced was dissolved

in a solution containing 1 ml of isopropanol, 4% HCl 1 N (left for 24 h at room temperature in dark conditions). Finally, the optical density (OD) was read against a reagent blank with multi well scanning spectrophotometer (ELISA reader, Asys Hitchech, Austria) at a wavelength of 570 nm. The cell viability was calculated using the following equation:

$$\text{Cell viability (\%)} = (A_{\text{treated}}/A_{\text{control}}) \times 100$$

where A_{treated} and A_{control} are the absorbance of the treated and untreated cells, respectively. The 50% cytotoxic concentration (C_{50}) was measured as the concentration of Pd(II) complexes at which 50% of the cells were viable compared with that of the control (23).

Biochemical Studies

All experiments involving the interaction of the complexes with ct-DNA were carried out in Tris-HCl buffer of pH 7.4 medium containing 10 mmolL^{-1} sodium chloride (24,25). The stock solutions of Pt(II) and Pd(II) complexes (5 mmolL^{-1}) were made in this medium by gentle stirring and heating at $35 \text{ }^{\circ}\text{C}$, while that of DNA (4 mg/mL) at $4 \text{ }^{\circ}\text{C}$ until homogenous. The metal complex solutions, with and without DNA were incubated at $27 \text{ }^{\circ}\text{C}$ and $37 \text{ }^{\circ}\text{C}$, separately. Then, the spectrophotometric readings at λ_{max} , 321, 309, 318 and 314 nm, for $[\text{Pt}(\text{bpy})(\text{But-gly})]\text{NO}_3$, $[\text{Pd}(\text{bpy})(\text{But-gly})]\text{NO}_3$, $[\text{Pt}(\text{bpy})(\text{Hex-gly})]\text{NO}_3$ and $[\text{Pd}(\text{bpy})(\text{Hex-gly})]\text{NO}_3$, respectively, where DNA has no absorption were measured. Using trial and error method, the incubation time for solutions of DNA-metal complexes at $27 \text{ }^{\circ}\text{C}$ and $37 \text{ }^{\circ}\text{C}$ found to be 2.5 h. No further changes were observed in the absorbance reading after longer incubation. The concentration of DNA was determined spectrophotometrically using a molar absorptivity of $6600 \text{ Lmol}^{-1} \text{ cm}^{-1}$ (258 nm) (26). Different techniques to probe the changes on DNA structure induced by complexes have been used:

Electronic absorption titration

Electronic absorption spectroscopy is universally employed to determine the binding parameters (n , K , g) of metal complexes with DNA as reported earlier (11, 27). Where n is the Hill coefficient, g is the number of binding sites per 1000 nucleotides of DNA and K is apparent binding constant. Also, the other thermodynamic binding parameters: molar Gibbs free energy of binding (ΔG_b°), molar enthalpy of binding (ΔH_b°) and molar entropy of binding (ΔS_b°) were determined according to reported method (14). All

measurements were performed separately at 27 °C and 37 °C and repeated three times for each complex.

Denaturation of DNA with Pt(II) and Pd(II) complexes

The application of UV absorption method to the study of denaturation of DNA with Pt(II) or Pd(II) complexes were similar to that reported earlier (14). In these studies, the concentration of each metal complex at midpoint of transition, $[L]_{1/2}$, was determined. Also, thermodynamic parameters such as: $\Delta G^\circ_{(H_2O)}$, conformational stability of DNA in the absence of metal complex; $\Delta H^\circ_{(H_2O)}$, the heat needed for DNA denaturation in the absence of metal complex; $\Delta S^\circ_{(H_2O)}$, the entropy of DNA denaturation by metal complex as well as m , measure of the metal complex ability to denature DNA were found out using Pace method (14,28,29). All measurements were performed in 0.01 molL⁻¹ Tris-HCl buffer (pH 7.4) at 27 °C and 37 °C, separately.

Modes of binding

The modes of binding of some platinum (II) and palladium (II) complexes with ct-DNA were done by the gel filtration, ethanol precipitation, electronic absorption and fluorescence experiments as reported earlier (11,30). The modes of binding between DNA and the above synthesized complexes were investigated by gel filtration experiments. G-25 Sephadex can be used for separation of double-stranded DNA fragments. The exclusion limits for 10 base pairs. For preparation of the column chromatograph, G-25 sephadex is placed in the usage buffer and allowed to swell for at least 3 h at 20 °C. The slurry mixture is poured into the column chromatograph in continuous motion to 20 ml void volume of the gel filtration column. Then, the column was filled to the top with buffer.

Fluorescence studies

Ethidium bromide (EB), one of the most sensitive fluorescence probes having a planar structure binds DNA by intercalative mode (31,32). At first, DNA (60 μmolL^{-1}) was added to 2 μmolL^{-1} aqueous ethidium bromide solution (3.7 μL DNA + 16 μL EB + 430.3 μL buffer) and maximum quantum yield for ethidium bromide was achieved at 471 nm, so we selected this wavelength as excitation radiation for all of the samples at different temperatures (27 °C and 37 °C) in the range of 540-700 nm. The widths of the excitation and the emission slit were set at 5.0 nm. To this solution (containing EB and DNA) different concentrations of the Pt(II) or Pd(II) complex (0.4, 0.5 and 0.6 mmolL⁻¹

¹) were added. The fluorescence intensities of the Pd(II) and Pt(II) complexes at the highest denaturant concentration at 471 nm excitation wavelength have been checked and the emissions intensities of these compounds were very small and negligible.

Molecular dynamic simulation

The structures of butyl- and hexyl-glycine derivatives were drawn using HyperChem 7 software, pre-optimized with Molecular Mechanics Force Field (MM+), and their final geometries were obtained with the semi-empirical AM1 method. Their force field parameters were generated using PRODRG2 server (33). The starting conformation for the simulations of the DNA was obtained from the protein data bank (PDB) structure 453D (34). The DNA was solvated with a mixture of five butyl- or hexyl-glycine derivatives and TIP3P water and placed in a cubic large enough boxes to contain the DNA and 1 nm of solvent on all sides. Molecular dynamics simulation was performed using GROMACS software version 3.3.1 (35). AMBER 01 force field was used to model atomic interactions (36). In all simulations, temperature was kept close to the intended values (27 °C and 37 °C) by using the Nose-Hoover algorithm (37). Pressure was also kept constant at 1 bar by applying Parrinello-Rahman algorithm (37). Leap-Frog integration algorithm was used to solve the motion equation by a time step of two femtoseconds. All bonds, including hydrogen bonds, were constrained by using LINCS algorithm (37). Electrostatic interactions between charged groups within 1.5 nm were calculated explicitly, while long-range electrostatic interactions were calculated using the Particle-Mesh Ewald (PME) method (38). Lenard-Jones and van der Waals's interactions were calculated with a 1.5 nm range cutoff. Grid algorithm was used to search neighbors (39). Table I lists a summary of the simulations. All the simulations were equilibrated by 1 ns with position restraints on the DNA and complex to relax solvent molecules. After equilibration, the molecular dynamic was run for 20 ns.

Production runs of all the systems were obtained three times to check repeatability and analyses were averaged from all three independent trajectories. To estimate the affinity of complex in binding to DNA, relative binding free energy is calculated for each complex using semi empirical linear interaction energy (LIE) methodology introduced by Aqvist et al ($\Delta G_{\text{binding}} = \alpha (\langle V_{\text{l-s}}^{\text{vdw}} \rangle_{\text{bound}} - \langle V_{\text{l-s}}^{\text{vdw}} \rangle_{\text{free}}) + \beta (\langle V_{\text{l-s}}^{\text{el}} \rangle_{\text{bound}} - \langle V_{\text{l-s}}^{\text{el}} \rangle_{\text{free}}) + \gamma$) (40).

Where $V_{\text{bound}}^{\text{el}}$ and $V_{\text{bound}}^{\text{vdw}}$ are the electrostatic and van der Waals interaction energies between the ligand and the solvated DNA from a molecular dynamics (MD) trajectory

with ligand bound to DNA and $V_{\text{free}}^{\text{el}}$ and $V_{\text{free}}^{\text{vdw}}$ are the electrostatic and van der Waals interaction energies between the ligand and the water from another MD trajectory with the ligand in water. The angle bracket indicates Boltzmann average and the subscripts l and s refer to the complex and the surround, respectively. For several ligand-DNA systems, a set of values of $\alpha=0.5$ and $\beta=0.16$ and $\gamma=0$ was found to give good results (40). In order to obtain free energy of binding using this method, system No. 5-8 of Table I were established and computations were only tested for palladium complexes. The Lennard-Jones parameters for the palladium were taken from reference (41) and inserted manually and compared with parameters calculated from Gaussian software obtained with density functional theory (DFT) B3LYP method and 6-311++G(d,p) basis set (42).

Results and discussion

Cytotoxicity evaluation

The *in vitro* anti-tumor properties of Pt(II) and Pd(II) complexes with butyl- and hexyl-glycine were carried out with human tumor cell line K562 (23). In this experiment, the cell growth was measured after incubation of cells in the presence of compounds (from 0 to 250 μmolL^{-1}) to be tested at 37 °C for 24 h. In Figures 1 the cell growth (in %) versus concentration (μmolL^{-1}) of above complexes is represented. The 50% cytotoxic concentration (C_{50}) of each compound was determined $>96 \mu\text{molL}^{-1}$ and $30 \mu\text{molL}^{-1}$ for butylglycine-Pd(II) and -Pt(II) complexes and $>96 \mu\text{molL}^{-1}$ and $80 \mu\text{molL}^{-1}$ for hexylglycine-Pt(II) and -Pd(II) complexes respectively.

Moreover, the C_{50} value of cisplatin under the same experimental conditions was determined to be $154 \mu\text{molL}^{-1}$, which is higher than the four prepared complexes. However, the C_{50} values of these complexes are slightly higher than that of our analogous Palladium(II) amino acid derivative complexes reported earlier (23).

DNA Binding Studies

Evaluation of binding parameters

In metal complex-DNA titration experiments, the amount of free and bound complex was determined as follow:

The isothermal titration of each metal complex (25 μL of 1 mmolL^{-1} stock) with different concentrations of DNA (50-100 μL for butyl system and 150-300 μL of stock

for hexyl system) in total volume of 2 mL was performed by applying electronic absorption spectroscopy at 27 °C and 37 °C, separately. The change in absorbance when all binding sites on DNA were occupied by metal complex, ΔA_{\max} , was determined from the plot of $1/[\Delta A]$ Vs $1/[\text{DNA}]$, where $\Delta A = A_{\text{DNA}} + A_{\text{com}} - A_{\text{DNA-com}}$ and shown in Table II. These values were used to calculate the concentration of metal complex bound to DNA, $[\text{L}]_b = \Delta A \cdot [\text{L}]_t / \Delta A_{\max}$, and the concentration of free metal complex, $[\text{L}]_f = [\text{L}]_t - [\text{L}]_b$ and $v = [\text{L}]_b / [\text{DNA}]_t$, ratio of the concentration of bound metal complex to total [DNA] in the next experiment, that is, titration of fixed amount of DNA (50 mL of stock) with varying amount of each metal complex (50-100 μL for butyl system and 150-300 μL of 1 mmolL^{-1} stock for hexyl system) in total volume of 2 mL at 27 °C and 37 °C, separately.

Using these data (v and $[\text{L}]_f$), the Scatchard plots were constructed for the interaction of each metal complex at the two temperatures 27 °C and 37 °C. The Scatchard plots are shown in Figures 2A for $[\text{Pt}(\text{bpy})(\text{but-gly})]\text{NO}_3$ and the insert for $[\text{Pd}(\text{bpy})(\text{but-gly})]\text{NO}_3$ and 2B for $[\text{Pt}(\text{bpy})(\text{Hex-gly})]\text{NO}_3$ and the insert for $[\text{Pd}(\text{bpy})(\text{Hex-gly})]\text{NO}_3$. These Scatchard plots are almost curvilinear concave downwards, suggesting positive cooperative binding (for determining binding parameters with minimum error, two final experimental points in curve at high v ratio were eliminated) (27). To obtain the binding parameters, the above experimental data (v and $[\text{L}]_f$) were substituted in Hill equation, $[v = g(K[\text{L}]_f)^n / (1 + (K[\text{L}]_f)^n)]$, to get a series of equation with unknown parameters n , K and g . Using Eureka software, the theoretical values of these parameters could be deduced. The results are tabulated in Table II which are comparable with those of 2,2'-bipyridine-platinum and -palladium complexes of dithiocarbamate as reported earlier (43-46).

The maximum errors between experimental and theoretical values of v are also shown in Table II which is quite low. The K , apparent binding constant and n , the Hill coefficient in the interaction of hexyl-glycine-Pt or -Pd complexes with DNA is higher than that of butyl-glycine-Pt or -Pd complexes with DNA (see Table II). Moreover, these data indicate that the cooperativity of $[\text{Pd}(\text{bpy})(\text{Hex-gly})]\text{NO}_3$ is more than $[\text{Pt}(\text{bpy})(\text{Hex-gly})]\text{NO}_3$. This may be because palladium complexes are about 10^5 times more labile than their platinum analogs (44). Moreover, finding the area under the sigmoidal binding isotherm curves (the values of v were plotted versus the values of Ln

$[L]_f$) and using Wyman-Jons equation (27), the K_{app} , ΔG°_b and ΔH°_b at 27 °C and 37 °C for each compound with DNA could be calculated. Plots of the values of ΔH°_b versus the values of $[L]_f$ are shown in Figures 3 for Pt complexes and the insert for Pd complexes at 27 °C. Deflections are observed in all plots. These deflections indicate that at particular $[L]_f$, there is a sudden change in enthalpy of binding which may be due to binding of metal complex to DNA or DNA denaturation. Similar observations can be seen in the literature where Pd(II) complexes interact with proteins (27,14).

Thermodynamic parameters in denaturation studies

The maximum unfolding of DNA by interaction with above platinum and palladium complexes occurs when all binding sites are occupied. In this experiment, the sample cell was filled with 1.8 mL Tris-HCl buffer containing $\sim 0.07 \text{ molL}^{-1}$ DNA for Pd(II) complexes and $\sim 0.09 \text{ molL}^{-1}$ DNA for Pt(II) complexes where absorption of these solutions are ~ 0.5 and ~ 0.7 , respectively. However, reference cell was filled with 1.8 mL Tris-HCl buffer only. Both cells were set separately at constant temperature of 27 °C or 37 °C and then 15 μL of Pt(II) or Pd(II) complex from stock solutions was added to each cell. After 3 min., the absorption was recorded at 258 nm for DNA and at 640 nm to eliminate the interference of turbidity. Addition of metal complex to both cells was continued until no further changes in the absorption readings were observed. The profiles of denaturation of DNA by Pt- and Pd-butyl-glycine and Pt and Pd-hexyl-glycine at two temperatures of 27 °C and 37 °C are shown in Figures 4A and 4B, respectively. The concentration of metal complexes in the midpoint of transition, $[L]_{1/2}$, for Pt(II) and Pd(II) complexes at 27 °C and 37 °C are shown in Table III. The important observation of this work is the low values of $[L]_{1/2}$ for these complexes (26,31,47) i.e. all the complexes (in particular $[\text{Pd}(\text{bpy})(\text{Hex-gly})]\text{NO}_3$) can denature DNA at low concentrations ($\sim 180\text{-}610 \mu\text{M}$). Thus, if these complexes will be used as anti-tumor agents, low doses will be needed, which may have fewer side effects.

Another significant observation of this work is the type of denaturation plots shown in figure 4. The inserts of fig.4A and 4B show ascending sigmoidal curves for both Pd(II) complexes. These results indicate the ability of both Pd(II) complexes to separate the two strands of the parent DNA resulting exposure of purine and pyrimidine bases to UV-light and hence absorption increases. However, the analogous Pt(II) complexes (fig 4A and 4B) exhibit descending sigmoidal denaturation curves which is probably because the winding the parent duplex DNA resulted in its precipitation. Thus the

difference in the interaction behavior of these analogous complexes may be due to the kinetics of central metal ions in the structure of them. Incidentally, palladium(II) complexes react about 10^5 - 10^6 times faster than platinum(II) complexes giving reaction rate that are too fast and may causes winding and hence precipitating the DNA.

Furthermore, some thermodynamic parameters found in the process of DNA denaturation are discussed here: The standard Gibbs free energy of DNA denaturation, ΔG° (the work needed for DNA denaturation) was calculated as a function of complex concentration by assuming two-state mechanism and using the equations $K = [A_N - A_{obs}] / [A_{obs} - A_D]$ and $\Delta G^\circ = -RT \ln K$, where A_{obs} is the observed absorbance used to follow unfolding in the transition region, A_N and A_D are the values of absorbance to the native and denatured conformations of DNA, respectively. The free energy of unfolding is calculated based on the data in the Fig. 4, which varies linearly with complex concentration in the transition region (28). A straight line with formula of $\Delta G^\circ = \Delta G^\circ_{H_2O} - m[\text{complex}]$ is obtained when the values of ΔG° are plotted versus the concentrations of each metal complex in the transition region at 27 °C and 37 °C. These plots are shown in Figures 5 for Pt(II) and the insert for Pd(II) systems. The m , slope of these plots (a measure of the metal complex ability to denature DNA) and the intercept on ordinate, $\Delta G^\circ_{(H_2O)}$, (conformational stability of DNA in the absence of metal complex) are summarized in Table III. Similar values have been observed for DNA denaturation with dithiocarbamate (43-45). Also, the values of ΔG° (see Table III) are decreased by increasing the temperatures for all complexes. This is as expected because in general, most of the macromolecules are less stable at higher temperature. The values of m for Pd(II)-hexyl-glycine complex are more than that of other three systems which indicate the higher ability of $[\text{Pd}(\text{bpy})(\text{Hex-gly})]\text{NO}_3$ to denature DNA.

Another important thermodynamic parameter found is the molar enthalpy of DNA denaturation in absence of metal complexes i.e. $\Delta H^\circ_{(H_2O)}$. For this, we calculated the molar enthalpy of DNA denaturation in presence of each metal complex, $\Delta H^\circ_{\text{conformation}}$ or $\Delta H^\circ_{\text{denaturation}}$, in the range of the two temperature using Gibbs-Helmholtz equation ($\Delta H^\circ = (\Delta G^\circ_{(T_1)}/T_1 - \Delta G^\circ_{(T_2)}/T_2) / (1/T_1 - 1/T_2)$) (48). On plotting the values of these enthalpies versus the concentrations of each metal complex, straight lines will be obtained which are shown in Figures 6. Intrapolation of these lines (intercept on ordinate i.e. absence of metal complex) give the values of $\Delta H^\circ_{(H_2O)}$ (see Table III).

Figure 6 shows that in the range of 27 °C to 37 °C the changes in the enthalpies in the presence of Pt(II)- and Pd(II)-hexyl-glycine complexes and Pt(II)-butyl-glycine are descending while that of Pd(II)-butyl-glycine is ascending. These observations indicate that on increasing the concentration of three first complexes, the stability of DNA is decreased while in the case of [Pd(bpy)(but-gly)]NO₃ the opposite trend was observed which may be due to low tendency of interaction of Pd(II)-butylglycine than other complexes with DNA. In addition, the entropy ($\Delta S^\circ_{(H_2O)}$) of DNA unfolding by Pt(II) and Pd(II) complexes have been calculated using equation $\Delta G^\circ_{(H_2O)} = \Delta H^\circ_{(H_2O)} - T\Delta S^\circ_{(H_2O)}$ and the data are given in Table III. These data show that the metal-DNA complex is more disordered than that of native DNA, because ΔS° is positive and ΔG° is negative and finally complex binding to DNA is a spontaneous process (see Table III). These data again show that ability of the hexyl-glycine systems in the denaturation of DNA is more than that of the butyl-glycine systems.

Evaluation of binding modes

In this evaluation, at first, a solution of DNA was passed through a Sephadex G-25 column and each eluted fraction of 2 ml was monitored spectrophotometrically at 258 nm to detect the DNA coming out and the absorption readings were plotted versus eluted fractions to construct chromatogram. Numbers of peaks in the chromatogram indicate the number of DNA fractions. When DNA alone is passed through column, a single peak is observed Figures 7A and 8A. Then, the solution of each interacted DNA-metal complex, 350 μ L of stock solution complex and 50 μ L DNA of stock solutions in 2.5 mL buffer (0.7 molL⁻¹ complex and 0.175 molL⁻¹ DNA) was passed through a Sephadex G-25 column equilibrated with the same buffer. Elution was done with buffer and each fraction of the column was monitored spectrophotometrically at λ_{max} of each complex (see Table II) and 258 nm for all systems for detecting DNA. The gel chromatograms obtained from these experiments are given in Figures 7 for Pt(II)- and Pd(II)-butyl-glycine complexes and Figures 8 for Pt(II)- and Pd(II)-hexyl-glycine complexes. These results show that the two peaks obtained at two wavelengths were not clearly resolved which indicate that metal complexes have not separated from DNA and their binding with DNA is strong enough that not readily break (43-46). Moreover, all four complexes break the DNA into two fractions, one smaller (left) and the other larger (right) and complexes interact with both factions because, in both peaks of

chromatograms, absorptions due to DNA (at 258 nm) and λ_{max} of complexes (see Table II) were observed.

Fluorescence titration studies

The fluorescence of ethidium bromide (EB) increases after intercalating in DNA. If the complex intercalates into DNA, it leads to a decrease in the binding sites of DNA available for EB-DNA system (31,32,49). The changes of fluorescence emission of intercalated EB in DNA with increasing concentrations of Pd(II) and Pt(II) complexes at 27 °C are shown in figures 9. These figures show a slowly reduction of the ethidium intensity by adding the different concentrations of each complex. (Similar observations were made at 37 °C). These results suggest that the above metal complexes presumably bind to DNA and provide conformation changes in it. As a result of these conformational changes some of EB molecules could not fit in the intercalation sites properly and thus fluorescence intensity of DNA intercalated EB is quenched.

Further, studies to characterize the mode of binding of Pd(II) complexes to ct-DNA were supported using fluorescence Scatchard analysis (50). Saturation curves of the fluorescence intensity for a series of DNA-Pt(II)/Pd(II) complexes, at increasing concentrations of each complex (0.3, 0.4 and 0.5 mmolL⁻¹) are obtained by adding increasing concentrations of EB (2,4,.. 20 μmolL^{-1}). The binding isotherms for the interaction of metal complexes are represented as fluorescence Scatchard plots ($r/[L]_f$ against r) and are given in Figures 10. In $r/[L]_f = nK_a - rK_a$ formula, r is the moles of EB bound per mole of DNA, $[L]_f$ is the molar concentration of the free EB, n is the number of binding sites per nucleotide and K_a is the apparent binding constant. The complexes show non-competitive inhibition of EB binding (Type-D behavior), in which the slope that is K_a with no change in the presence of increasing amounts of metal complexes, with decreases in the intercept on the abscissa that is n (51). This implies that all complexes are bound to DNA via hydrogen and groove binding but not intercalation.

Molecular Dynamics Simulation

We first analyzed the root mean square deviation of DNA in the butyl and hexyl derivatives at two temperatures. In Figure 11A, the Root mean square deviation (RMSD) of systems was calculated at two temperatures. As found, DNA square deviation is more at higher temperatures and in butyl complex. In this work the RMSD rises almost continuously over the first 4 ns. In butyl complex and at 310 K, the RMSD

overcomes 3.5 nm and the most structure deviation is observed. Figure 11B shows averaged solvent accessible surface area of DNA in 20 ns time interval in the presence of butyl and hexyl derivatives at 27 °C and 37 °C. This figure shows more increase of surface in the presence of butyl at 37 °C. It is obvious that DNA structure is unfolding and average surface area of DNA in system with butyl at 37 °C is increased more. Figure 11C shows the averaged gyration radius (R_g) of DNA in 20 ns time interval and it confirms gyration radius of DNA increase at higher temperatures and in the presence of butyl derivative. This result is in good accordance with increase of surface area of DNA. This shows that the DNA structure has been unfolded and denatured more in butyl system at 37 °C.

Figure 12A and 12B show the average intermolecular hydrogen bonds (H-B) and hydrogen bonds between the DNA and solvent over the course of the MD simulations. The total number of hydrogen bonds between DNA and water and intermolecular hydrogen bond decrease with temperature and in butyl derivative. These data suggest that the butyl molecules attach themselves to the DNA better than hexyl derivative at higher temperatures, and the solvent-DNA hydrogen bonds are replaced by DNA-butyl hydrogen bonds. Thus, the interaction between the DNA and butyl molecules are thought to stabilize the denatured state and lead to DNA denaturation and as a result of denaturation, intermolecular hydrogen bond decreases. We have calculated atomic radial distribution functions (RDF) to compare the strength of direct interactions between DNA and complex. The radial distribution function of DNA-complex presented in Figure 12C confirms more attach of butyl derivative to DNA. The strength of RDF profile (denoted by $g(r)$) at higher temperatures and in the presence of butyl is higher compared to the $g(r)$ magnitude in hexyl. Thus, butyl interacts more strongly with the DNA than water, suggesting that accumulation of butyl around the DNA causes poor solvation of the DNA and unfolding of structure. The present work suggests that the number of hydrogen bonds between DNA and with water decreases with time but this decrease is more prominent at higher temperatures and in butyl comparing to hexyl derivative.

Results of $g(r)$ of complex-solvent (Figure 13A) shows that RDF decreases by temperature in the presence of butyl derivative. It reveals that butyl is excluded from solvent surface. In order to explain this phenomenon, we have used gradual hydration and repulse concepts at lower temperatures and in the presence of hexyl derivative.

Results show that solvent molecules are increased in hydration layer around DNA and this is due to hexyl molecules that go away from DNA surface. We can conclude from $g(r)$ diagrams that a thin hydration layer is formed on DNA surface in lower temperatures in the presence of hexyl derivative. The $g(r)$ of solvent around DNA versus distance is shown in Figure 13B. At high temperatures, butyl derivative exclude solvent away from DNA more and this result is in good agreement with hydrogen bond results. As a consequence, both complexes cause solvent exclusion from DNA and this effect is higher for butyl due to its less steric hindrance and hydrophobic property.

Time-coursed snapshots of the butyl system at 27 °C depicted in Figure 14 indicate interaction of butyl with the DNA. During the simulation, the butyl came near the DNA and it began to bind the DNA via groove binding at the time of 20 ns which is indicated by an orange circle.

A number of papers have shown LIE as a method with fast and reliable estimates of binding free energies (52,53). Table IV presents the difference in average interaction energies (free energies) of complex and DNA. When the ligand locates far from DNA, the Gibbs free energy is less negative and the value rapidly decreases after the ligand interacting with DNA or after binding to DNA. This result is in good accordance with those obtained from previous studies. According to previous studies, negative free energy confirms that the ligand prefers to bind to the DNA. The most negative value of free energy is at higher temperatures and in the presence of butyl derivative. Equilibrium of system has been monitored by quantities such as temperature and pressure of the systems presented in Table V. The steady state in these parameters confirms equilibrium in NPT ensemble indicating that all systems can be used for subsequent data sampling. Also, bond lengths and force constant (Table VI) were obtained from quassian software, then needed parameters for palladium were calculated from them.

Conclusion

In summery, cytotoxic Data show that the CC_{50} values of Pt(II) and Pd(II) complexes are lower than cisplatin which indicating of the more cytotoxicity and anti-cancer activity of these compounds. Maybe the presence of glycinato moiety with hydrophobic tail in the structure of metal complexes has great influences on the growth suppression activity of these complexes on K562 cells. Also, the experimental binding results taken together indicate that all complexes cooperatively interacted with DNA at low concentration in

the mode of hydrogen or van der Waals binding and presumably groove binding. Molecular dynamics simulation results show that hydrogen bond interactions between butyl molecules and the DNA, solvent accessible surface area of DNA and the radius of gyration of DNA vary with temperature and complex. The direct relationship between these parameters and hydrophobicity of complex is the dominant mechanism by which the DNA is unfolded at higher temperatures. The butyl molecules interact and bind strongly to the DNA via groove binding and have the most negative value of binding free energy. This strong binding and interaction confirmed by RDF data leads to the unfolding of DNA. Finally we find that with the decreasing of hydrophobicity or steric hindrance of complex, the complexes tend to have groove binding interaction and eventually they can bind on the DNA surface stably. Trend and results of structural parameters of simulation was compatible with experimental results.

Acknowledgments

Financial assistance from the Research Council of Chemistry & Chemical Engineering Research Center of Iran and of University of Sistan and Baluchestan and University of Tehran are gratefully acknowledged.

References and notes

1. H. Sigel, *Metal Ions in Biological Systems*, Marcel Dekker, New York, vol.11, pp. 1-196 (1980).
2. A. S. Abu-Surrah, M. Kettunen, *Curr. Med. Chem.* *13*, 1337-1357 (2006).
3. V. Alverdi, L. Giovagnini, C. Marzano, R. Seraglia, F. Beltio, S. Sintran, R. Graziani, D. Fregona, *J. Inorg. Biochem.* *98*, 1117-1128 (2004).
4. N. J. Farrell, In *Catalysis by Metal Complexes*, B. R. James, R.Ugo (Eds.), vol.11, Kluwer Academic Publishers, Dordrecht, The Netherlands (1989).
5. N. Manav, A. K. Mishra, N. K. Kaushik, *Spectrochim. Acta A.* *60*, 3087-3092 (2004).
6. Y. E. Kwon, K. J. Whang, Y. J. Park, K. H. Kim. *Bioorg. Med. Chem.* *11*, 1669-76 (2003).
7. C. Marzano, A. Trevisan, L. Giovagnini, D. Fregona, *Toxicol. Vitro.* *16*, 413-9 (2002).

8. A.S. Abu-Surrah, H. H. Al-Sa'doni, M. Y. Abdalla, *Cancer Therapy*, *6*, 1-10 (2008).
9. M. P. M. Marques, *ISRN Spectroscopy*, *2013*, 1-29 (2013).
10. V. X. Jin, J. D. Ranford, *Inorg. Chim. Acta*, *304*, 38-44 (2000).
11. A. I. Anzellotti, M. Sabat, N. Farrell, *Inorg. Chem.* *45(4)* 1638-45 (2006).
12. A. A. Saboury, A. A. Shamsaei, A. A. Mosavi Movahedi, H. Mansouri-Torshizi, *J. Chin. Chem. Soc.* *46*, 917-922 (1999).
13. E. Agostinelli, M. P. M. Marques, R. Calheiros, F. P. S. C. Gil, G. Tempera, N. Viceconte, V. Battaglia, S. Grancara, A. Toninello, *Amino Acids*, *38(2)* 393-403 (2010).
14. H. Mansouri-Torshizi, M. Islami-Moghaddam, A. A. Saboury, *Acta Bioch. Bioph. Sin.* *35*, 886-890 (2003).
15. Mylonas, S.; Valavanidis, A.; Voukouvalidis, V.; *Inorg. Chim. Acta.* *55*, 125-128 (1981).
16. J. K. Barton, S. J. Lipard, *Heavy Metal interactions with nucleic acids*. T. G. Spiro (Ed.) *Metal Ions in Biology*. Vol. 1, New York, USA: Wiley- Interscience, 31-114 (1980).
17. R. N. Bose, S. K. Ghosh, S. Moghaddas, *J. Inorg. Biochem.* *65*, 199-205 (1997).
18. S. Moradell, J. Lorenzo, A. Rovira, S. V. Zutphen, F. X. Aviles, V. Moreno, R. de Llorens, M. A. Martinez, J. Reedijk, A. Llobet, *J. Inorg. Biochem.* *98*, 1933-46 (2004).
19. A. Divsalar, A. A. Saboury, H. Mansouri-Torshizi, A. A. Mosavi-Movahedi, *J. Biomol. Struct. Dyn.* *25*, 173-82 (2007).
20. S. A. Shaikh, S. R. Ahmed, B. Jayaram, *Arch. Biochem. Biophys.* *429*, 81-99 (2004).
21. B. O. Brandsdal, J. Aqvist, A. O. Smalas, *Protein Sci.* *10*, 1584-95 (2001).
22. F. A. Palocsay, J. V. Rund, *Inorg. Chem.* *8*, 524-528 (1969).
23. A. Divsalar, A. A. Saboury, R. Yousefi, A. A. Moosavi-Movahedi, H. Mansouri-Torshizi, *Int. J. Biol. Macro.* *40*, 381-386 (2007).
24. M. Eslami Moghadam, M. Saidifar, F. Rostami-Charati, D. Ajloo, M. Ghadamgahi, *Comb. Chem. High T. Scr.* *17*, 781-789 (2014).
25. M. Saeidifar, H. Mansouri-Torshizi, Y. Palizdar, M. Eslami-Moghadam, A. Divsalar, A. A. Saboury, *Acta Chim. Slov.* *61*, 126-136 (2014).
26. Z. H. Xu, F. J. Chen, P. X. Xi, X. H. Liu, Z. Z. Zeng, *J. Photochem. Photobiol A: Chem.* *196*, 77-83 (2008).

27. A. A. Saboury, *J. Iran. Chem. Soc.* 3, 1-21 (2006).
28. R. F. Greene, C. N. Pace, *J. Biol. Chem.* 249, 5388-5393 (1974).
29. S. Z. Bathaie, A. Bolhasani, R. Hoshyar, B. Ranjbar, F. Sabouni, A. A. Moosavi-Movahedi, *DNA and Cell Biol.* 26, 533-540 (2007).
30. R. Mital, N. Jain, T. S. Srivastava, *Inorg. Chim. Acta.* 166, 135-140 (1989).
31. L. Peres-Flores, A. J. Ruiz-Chica, J. G. Delcros, F. M. Sanches, F. J. Ramirez, *Spectrochim. Acta. Part A.* 69, 1089-1096 (2008).
32. A. G. Krishna, D. V. Kumar, B. M. Khan, S. K. Rawal, K. N. Ganesh, *Biochim. Biophys. Acta.* 1381, 104-112 (1998).
33. A. W. Schuttelkopf, D. M. F. van Aalten, *Acta Crystallogr.* 60, 1355-63 (2004).
34. <http://www.rcsb.org>.
35. D. Van Der Spoel, *J. Comput. Chem.* 26, 1701-1718 (2005).
36. M. G. Wolf, G. Groenhof, *J. comput. Chem.* 33, 2225-32 (2012).
37. G. Bussi, D. Donadio, M. Parrinello, *J. Chem. Phys.* 126, 14101-14107 (2007).
38. D. Fincham, *Mol. Sim.* 8, 165-178 (1992).
39. H. Gao, *Nano. Lett.* 3(4) 471-473 (2003).
40. J. Åqvist, C. Medina, J. E. Samuelsson, *Protein Eng.* 7, 385-91 (1994).
41. S. Erkoc, *Ann. Rev. Comput. Phys.* IX., 1, 1-103 (2001).
42. S. Jalili, A. Jaberli, M. G. Mahjani, M. Jafarian, *Molecular Physics: An International Journal at the Interface between Chemistry and Physics.* 110, 361-368 (2012).
43. H. Mansouri-Torshizi, M. I-Moghaddam, A. Divsalar, A. A. Saboury, *Bioorg. Med. Chem.* 16, 9616-9625 (2008).
44. M. Islami-Moghaddam, H. Mansouri-Torshizi, A. Divsalar, A. A. Saboury, *J. Iran. Chem. Soc.* 6(3) 552-569 (2009).
45. H. Mansouri-Torshizi, M. I-Moghaddam, A. Divsalar, A. A. Saboury, *J. Biomol. Struct. Dyn.* 26(5) 575-586 (2009).
46. H. Mansouri-Torshizi, M. Eslami Moghaddam, A. Divsalar, A. A. Saboury, *Acta Chim. Slov.* 58(4) 811-822 (2011).
47. P. X. Xi, Z. H. Xu, X. H. Liu, F. J. Cheng, Z. Z. Zeng, *Spectrochim. Acta. Part A: Mol. Biomol. Spectrosc.* 71, 523-8 (2008).
48. G. M. Barrow, *In Physical Chemistry*, chap. 7, 5th ed.; M.C. Graw-Hill, New York (1988).
49. J. L. Butour, J. P. Macquet, *Eur. J. Biochem.* 78, 455-463 (1977).

50. G. Scatchard, *N. Y. Ann, Acad. Sci.* *51*, 660-672 (1949).
51. M. Howe-Grant, K. C. Wu, W. R. Bauer, S. J. Lippard, *Biochemistry*, *15*, 4339-4346 (1976).
52. R. A. Nome, *J. Braz. Chem. Soc.* *21*, 2189-2204 (2010).
53. J. J. Tan, R. Kong, C. X. Wang, W. Z. Chen, *J. Mol. Struct. (THEOCHEM)*, *682*, 9-15 (2004).

Accepted Manuscript

Table I Summary of studied systems

No	system	No. water	T (°C)
1	DNA-[Pd(bpy)(Butylgly)]NO ₃	3968	27
2	DNA-[Pd(bpy)(Butylgly)]NO ₃	3968	37
3	DNA-[Pd(bpy)(hexylgly)]NO ₃	3910	27
4	DNA-[Pd(bpy)(hexylgly)]NO ₃	3910	37
5	[Pd(bpy)(Butylgly)]NO ₃	4248	27
6	[Pd(bpy)(Butylgly)]NO ₃	4248	37
7	[Pd(bpy)(hexylgly)]NO ₃	3967	27
8	[Pd(bpy)(hexylgly)]NO ₃	3967	37

Table II Values of ΔA_{\max} and binding parameters in the Hill equation for interaction between Pt(II) and Pd(II) complexes and DNA in 10 mmol/L Tris-HCl buffer and pH 7.4

Compound	Temperature	^a λ_{\max} (nm)	^b ΔA_{\max}	^c g	^d K (Lmol ⁻¹)	^e n	^f error
[Pt(bpy)(But-gly)]NO ₃	27° C	321	0.138	9	0.009	3.42	0.006
	37° C		0.062				9
[Pd(bpy)(But-gly)]NO ₃	27° C	306	0.097	9	0.017	4.39	0.066
	37° C		0.051				9
[Pt(bpy)(Hex-gly)]NO ₃	27° C	318	0.045	7	0.021	5.64	0.08
	37° C		0.019				7
[Pd(bpy)(Hex-gly)]NO ₃	27° C	314	0.022	7	0.048	2.17	0.06
	37° C		0.017				7

^a wavelengths monitored to detect complexes. In this region DNA has no absorption.

^b change in the absorbance when all the binding sites on DNA were occupied by each of the metal complexes.

^c the number of binding sites per 1000 nucleotides.

^d the apparent binding constant.

^e the Hill coefficient (as a criterion of cooperativity).

^f maximum error between theoretical and experimental values of v .

Table III Thermodynamic parameters of DNA denaturation by platinum (II) and palladium (II) complexes

Compound	Temperature	^a [L] _{1/2}	^b m	^c $\Delta G_{(H_2O)}^\circ$	^d $\Delta H_{(H_2O)}^\circ$	^e $\Delta S_{(H_2O)}^\circ$
[Pt(bpy)(But-gly)]NO ₃	27° C	0.29	74.2	21.6	117.2	0.32
	37° C	0.25	73.6	18.3		
[Pd(bpy)(But-gly)]NO ₃	27° C	0.41	63.5	26.1	56.5	0.1
	37° C	0.35	71.7	25.1		
[Pt(bpy)(Hex-gly)]NO ₃	27° C	0.55	55	33.64	223.4	0.63
	37° C	0.61	48	27.28		
[Pd(bpy)(Hex-gly)]NO ₃	27° C	0.24	104	20.7	177.5	0.52
	37° C	0.18	61	15.45		

^a The concentration of ligand in the midpoint of transition ($\mu\text{mol/L}$)^b measure of the metal complex ability to destabilize DNA ($\text{kJ/mol}(\text{mmol/L})^{-1}$)^c conformational stability of DNA in the absence of metal complex (kJ/mol)^d the entropy of DNA denaturation by metal complex (kJ/mol)^e the heat needed for DNA denaturation in the absence of metal complex (kJ/molK)

Table IV Free energy values of systems obtained from LIE method.

No	Bounded(kJ.mol ⁻¹)		free(kJ.mol ⁻¹)		Free Energy (kJ.mol ⁻¹)
	Electrostatic	VDW	Electrostatic	VDW	
1	42.67	-4495	-26.40	-4396	-38.84
2	49.85	-5914	-24.49	-5762	-64.05
3	-27.08	-4332	-68.92	-4299	-9.810
4	-75.29	-4227	-36.39	-4198	-20.74

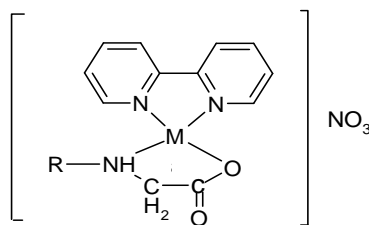
Table V. Temperature and pressure value of studied systems during simulation (No column is based on Table I numbering)

No	Temperature(°C)	Pressure (bar)
1	27.15	1.03
2	37.68	0.92
3	27.71	0.90
4	37.07	1.17

Table VI. Bond lengths and force constant of Pd with its neighbouring atoms according to scheme 1.

Atom number	Force constant(mDyn.A ⁻¹)	Bond length (A)
Pd- N ^a	1.92	1.93
Pd-O	1.94	1.88
Pd- N ^a	2.17	1.93
Pd- N ^b	1.19	1.96

^a Force constant and bond length of Pd-N of cyclohexene ring.^b Force constant and bond length of Pd-N of cyclopentane ring.

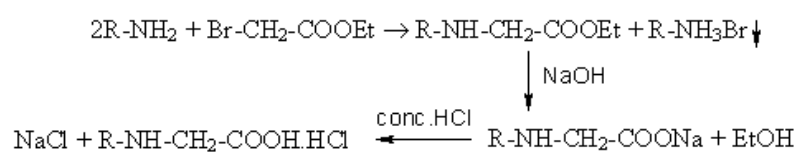


M= Pt(II) or Pd(II)

R= CH₃-(CH₂)_n-
n= 3, 5, 7

Scheme 1. Proposed structures of [M(bpy)(R-gly)]NO₃ (where M is Pt(II) or Pd(II), R-gly is butyl-, hexyl- or octyl-glycine and bpy is 2,2' bipyridine).

Accepted Manuscript



Scheme 2. General preparation route of the ligands R-Gly (R = butyl, hexyl or octyl).

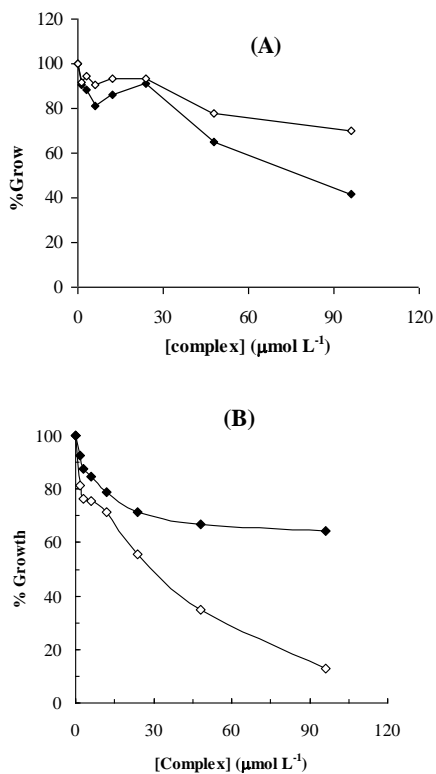


Figure 1. The growth suppression activity A) of the Pd(II)- (\diamond) and Pt(II)-butylglycine complex(\blacklozenge) and B) of the Pd(II)- (\diamond) and Pt(II)-hexyl-glycine complexes(\blacklozenge) on K562 cell line was incubated with varying concentrations of the complexes for 24 h.

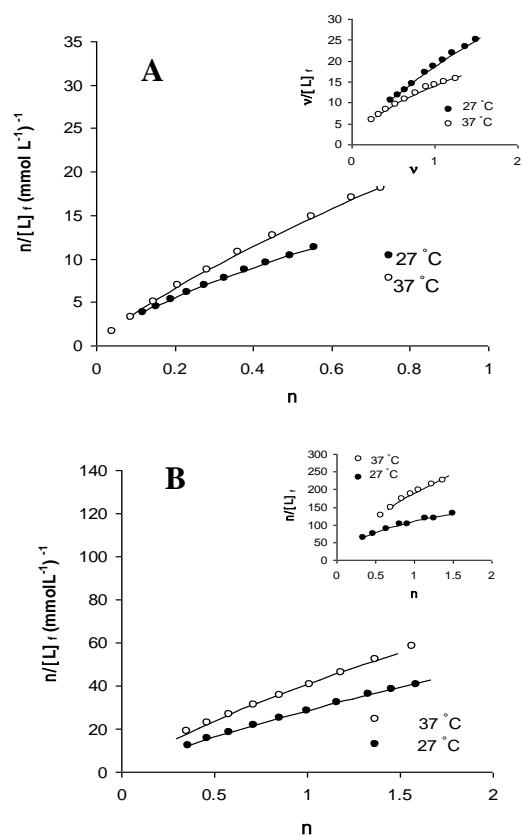


Figure 2. Scatchard plots for binding of A) Pt(II)-butyl-gly and B) Pt(II)-hexyl-gly with DNA. The inserts are Scatchard plots for binding of their Pd(II) analogs with DNA.

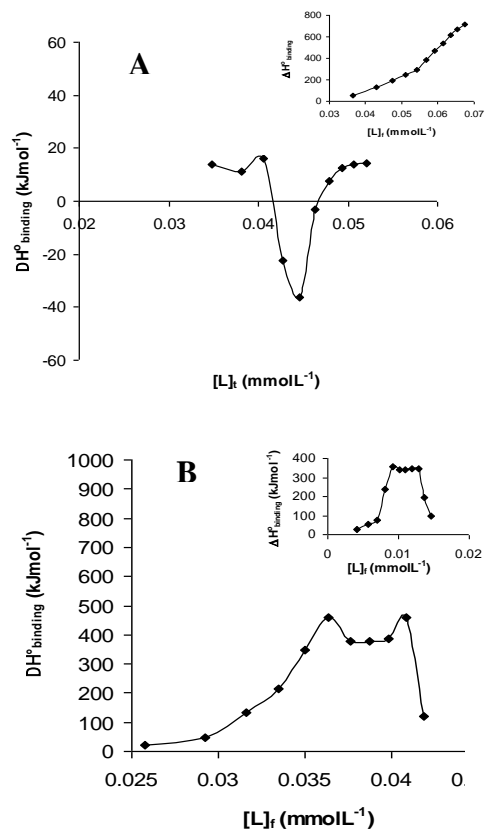


Figure 3. Molar enthalpies of binding in the interaction between DNA and A) Pt(II)-butyl-gly and B) Pt(II)-hexyl-gly (Inserts: Pd(II) systems) versus free concentrations of complexes at pH 7.4 and 27 °C.

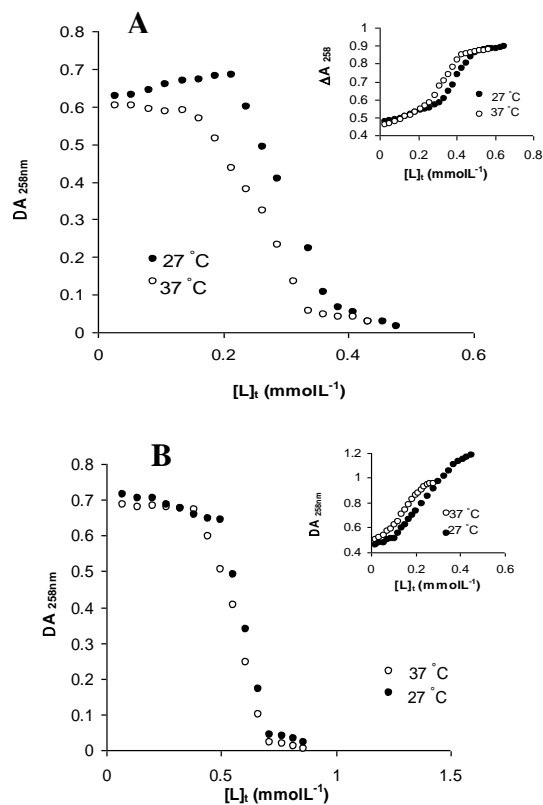


Figure 4. The DNA denaturation due to increasing the total concentration of A) Pt(II)-butyl-gly and B) Pt(II)-hexyl-gly (the inserts: their analogous Pd(II) systems) at constant temperatures of 27 °C and 37 °C.

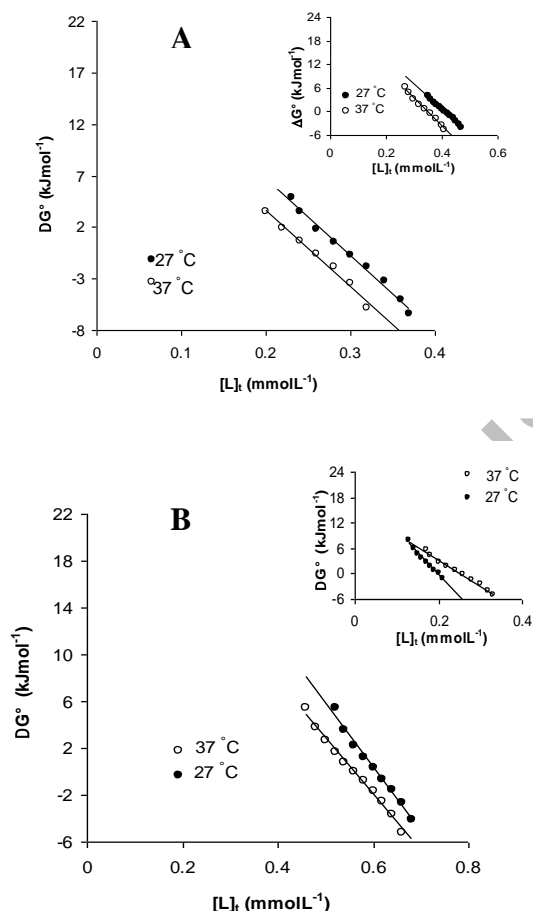


Figure 5. The molar Gibbs free energies plots of unfolding (ΔG° vs. $[L]_t$) of DNA in the presence of A) Pt(II)-butyl-gly and B) Pt(II)-hexyl-gly. Inserts: in the presence of analogous Pd(II) complexes.

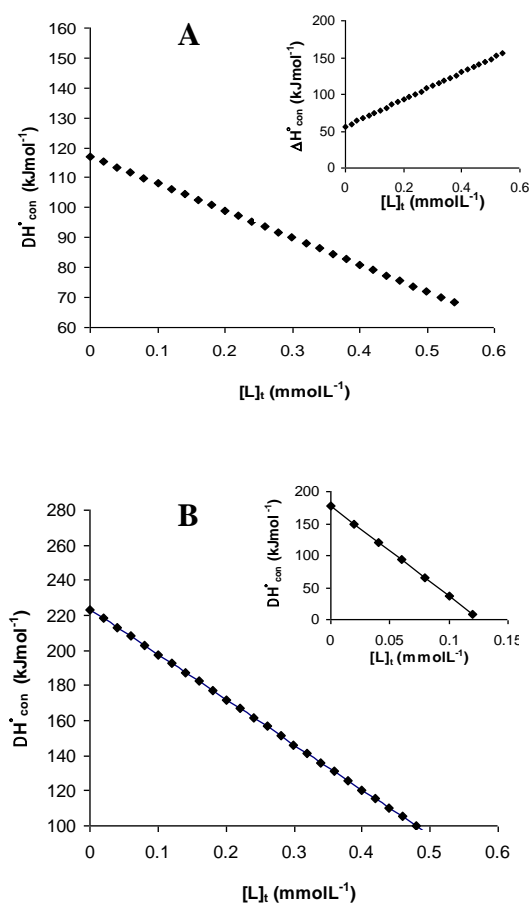


Figure 6. Plots of the molar enthalpies of DNA denaturation in the interaction with A) Pt(II)-butyl-gly and B) Pt(II)-hexyl-gly and the inserts with analogous Pd(II) complexes in the range of 27°C to 37°C.

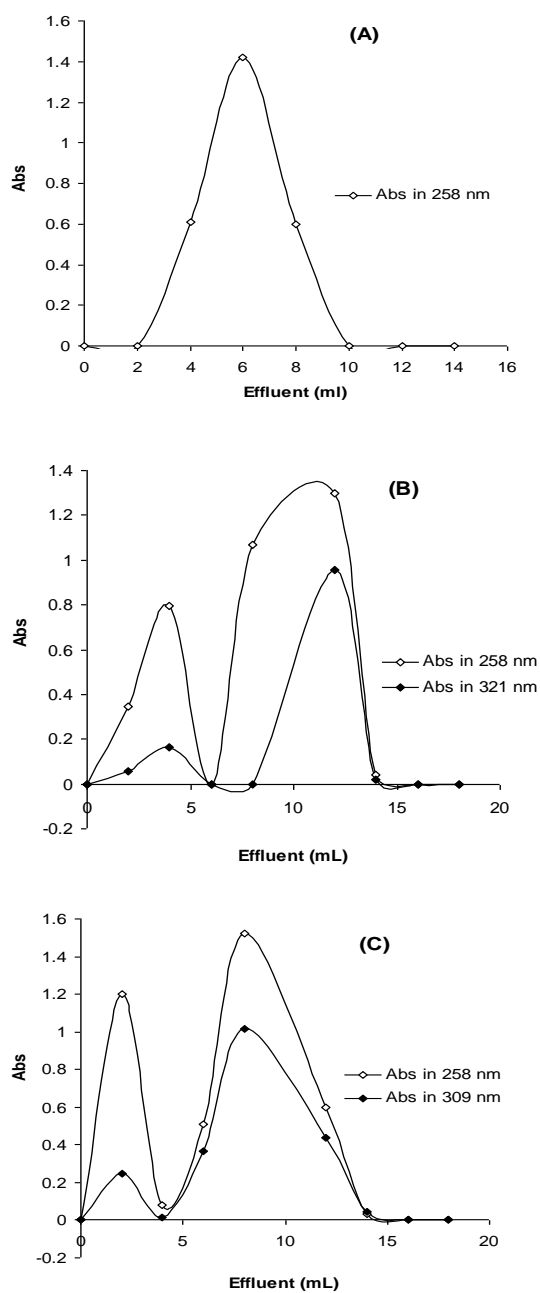


Figure 7. Gel chromatograms of free ct-DNA (A), [Pt(bpy)(but-gly)]NO₃-DNA complex (B) and [Pd(bpy)(but-gly)]NO₃-DNA complex (C), obtained on Sephadex G-25 column.

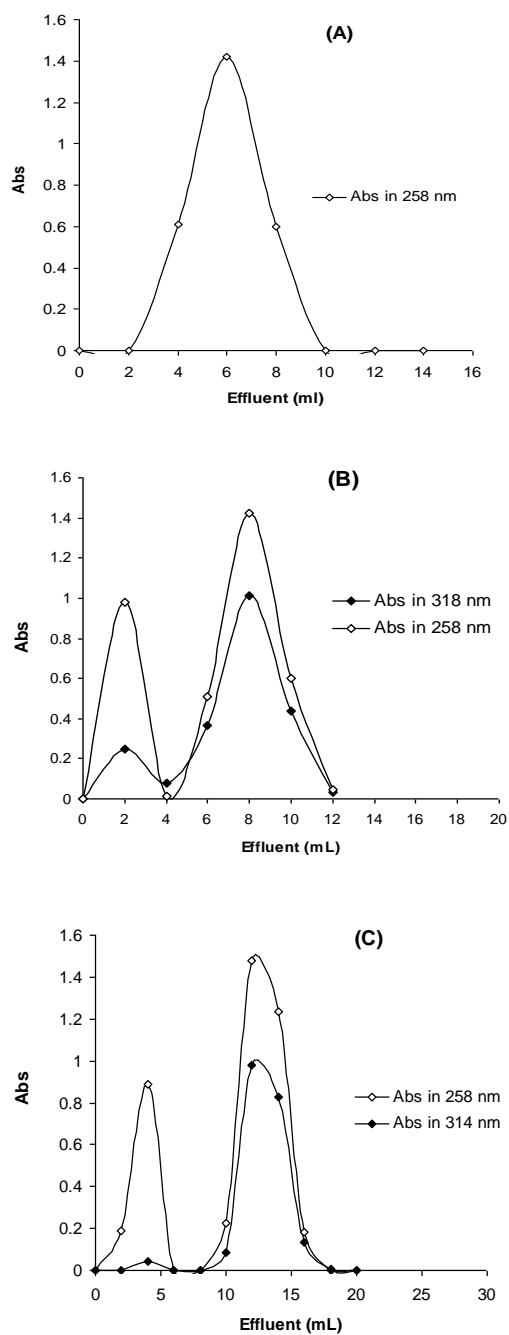


Figure 8. Gel chromatograms of free ct-DNA (A), [Pt(bpy)(hex-gly)]NO₃-DNA complex (B) and [Pd(bpy)(hex-gly)]NO₃-DNA complex (C), obtained on Sephadex G-25 column.

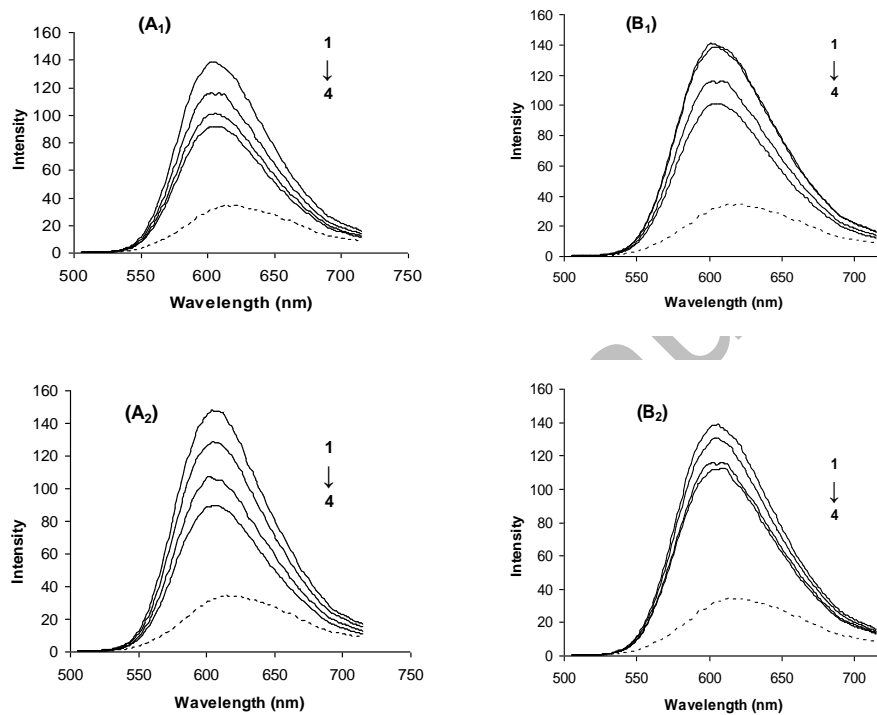


Figure 9. Fluorescence emission spectra of EB (dotted), EB bound to DNA in the presence of 0.3, 0.4 and 0.5 mM of: A₁) [Pt(bpy)(but-gly)]NO₃, B₁) [Pd(bpy)(but-gly)]NO₃, A₂) [Pt(bpy)(hex-gly)]NO₃ and B₂) [Pd(bpy)(hex-gly)]NO₃ at 27 °C.

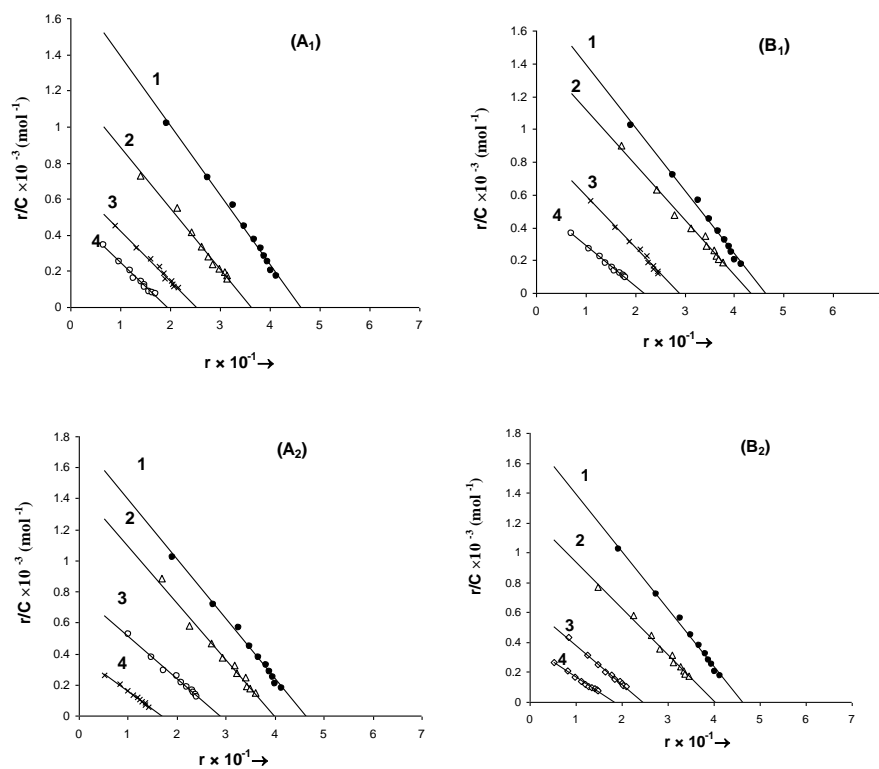


Figure 10. Fluorescence Scatchard plots for the binding of EB (2 to $24 \mu\text{molL}^{-1}$) to DNA ($60 \mu\text{molL}^{-1}$) in the absence of (line 1) and presence (line 2, 3 and 4) of increasing 300 , 400 and $500 \mu\text{molL}^{-1}$ of A₁) [Pt(bpy)(but-gly)]NO₃, B₁) [Pd(bpy)(but-gly)]NO₃, A₂) [Pt(bpy)(hex-gly)]NO₃ and B₂) [Pd(bpy)(hex-gly)]NO₃; r_f increases in the order of 0 (1), 5 (2), 6.6 (3) and 8.3 (4) in (A) and (B).

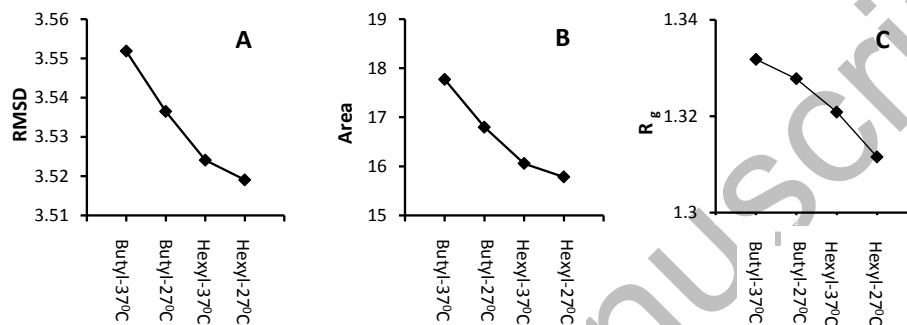


Figure 11. The averaged A) root mean square deviation, B) surface accessible area and C) gyration radius of the DNA with respect to the initial NMR structure for the simulations.

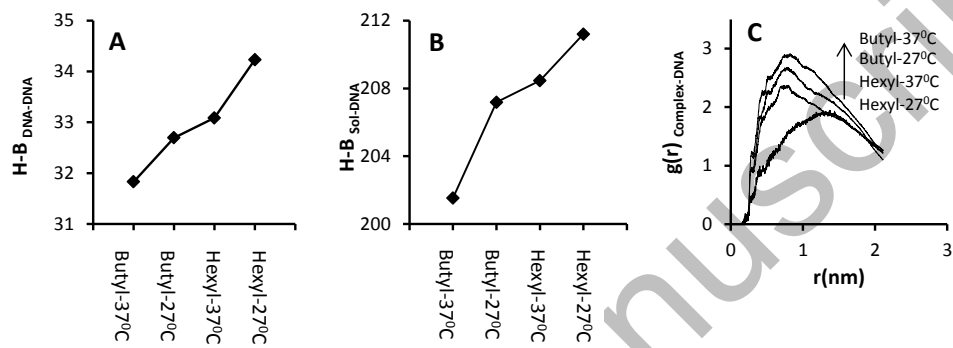


Figure 12. The total number of A) intermolecular H-Bs and B) H-B between sol-DNA and C) radial distribution function, $g(r)$ for complex around DNA.

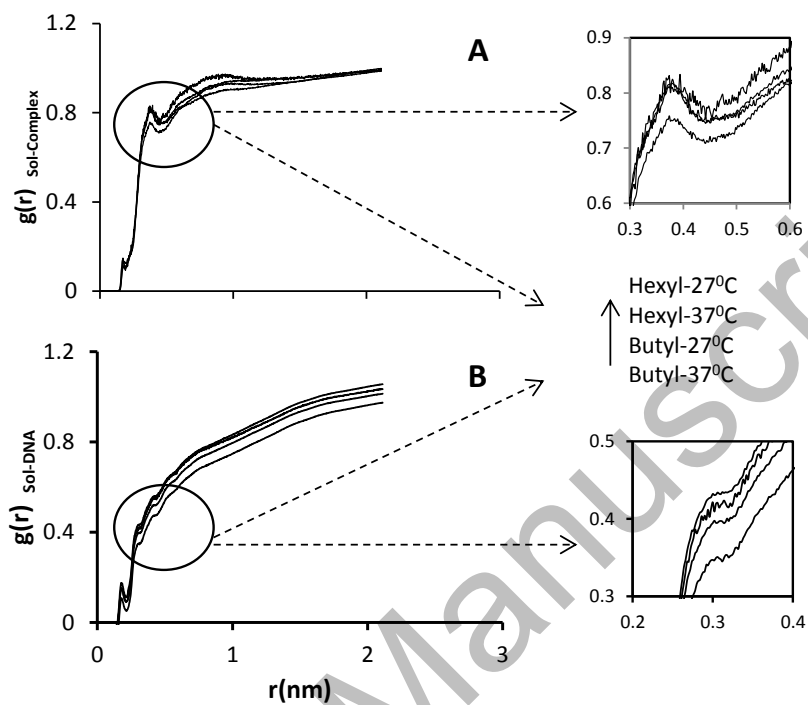


Figure 13. Calculated radial distribution function, $g(r)$ for (A) solvent around complex and (B) solvent around DNA.

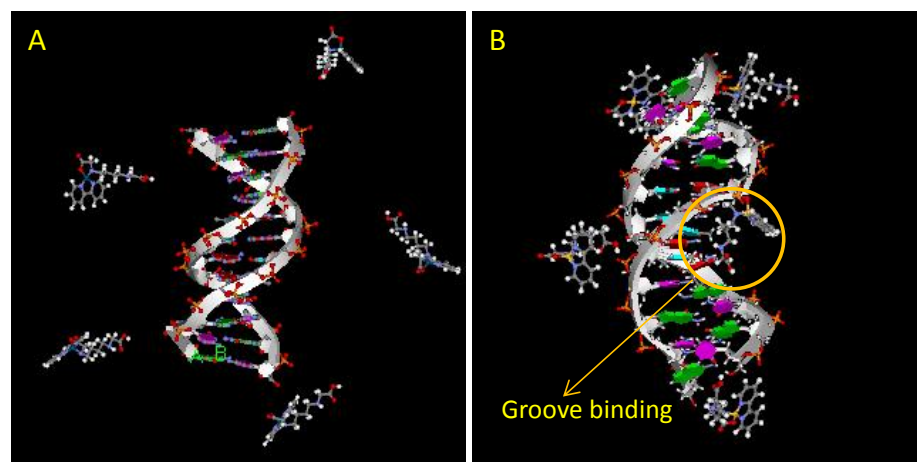


Figure 14. Snapshots from the MD simulations showing butyl system at 310 K A) before simulation and B) within 20 ns.

Graphical Abstract

Some anticancer Pt(II) and Pd(II) complexes of amino acid derivatives have been synthesized, characterized and interacted with calf thymus DNA. Their biological activities have been tested against leukemia cell line, K562. Modes of binding have been studied by electronic absorption, gel chromatography, fluorescence and other measurements. Simulation data indicates that the DNA structure largely maintains its native structure in hexylglycine derivative–water mixtures and at lower temperatures. More destabilizing effect of butylglycine induces by preferential accumulation and interaction of these molecules around the DNA via groove binding.

